Research Square

Preprints are preliminary reports that have not undergone peer review.
They should not be considered conclusive, used to inform clinical practice,
or referenced by the media as validated information.

Selenium-dependent Structural and Optoelectronic Properties of Mo-Free Cu 2 ZnSn(S,Se) 2 Solar Cells Prepared from Elemental Precursors

Eka Cahya Prima
ekacahyaprima@upi.edu
Universitas Pendidikan Indonesia
Ricky Aditya
Jenderal Achmad Yani University
Ermalinda Zebua
Universitas Pendidikan Indonesia
Ari Budiyanto
Universitas Pendidikan Indonesia
Arie Hardian
Jenderal Achmad Yani University
Endi Suhendi
Universitas Pendidikan Indonesia
Andhy Setiawan
Universitas Pendidikan Indonesia
Suyatman Suyatman
Institut Teknologi Bandung
Brian Yuliarto
Institut Teknologi Bandung

Research Article

Keywords: Solar cell, Kesterite, Non-vacuum fabrication, Element materials

Posted Date: September 29th, 2026

DOI: https://doi.org/10.21203/rs.3.rs-10487874/v1

License: This work is licensed under a Creative Commons Attribution 4.0 International License.
Read Full License

Additional Declarations: No competing interests reported.

Selenium-dependent Structural and Optoelectronic Properties of Mo-Free $Cu_2ZnSn(S,Se)_2$ Solar Cells Prepared from Elemental Precursors

Eka Cahya Prima[1]*, Ricky Aditya[1,2], Ermalinda Zebua[1], Ari Budiyanto[1], Arie Hardian[2], Endi Suhendi[3], Andhy Setiawan[3], Suyatman[4], Brian Yuliarto[4,5]

[1]Solar Energy Materials Laboratory, Department of Science Education, Faculty of Mathematics and Science Education, Universitas Pendidikan Indonesia, Bandung 40154, Indonesia
[2]Department of Chemistry, Faculty of Sciences and Informatics, Jenderal Achmad Yani University, Bandung 40531, Indonesia
[3]Materials Physics Laboratory, Department of Physics, Faculty of Mathematics and Science Education, Universitas Pendidikan Indonesia, Bandung 40154, Indonesia
[4]Advanced Functional Materials Laboratory, Faculty of Industrial Engineering, Institut Teknologi Bandung, Bandung 40132, Indonesia
[5]Research Center for Nanosciences and Nanotechnology, Institut Teknologi Bandung, Bandung 40132, Indonesia

*Corresponding e-mail address: ekacahyaprima@upi.edu

Abstract. Indonesia is located in the Ring of Fire, which produces abundant mineral resources suitable for research on solar cell materials. CZTS thin-film solar cells are believed to compete with silicon solar cells due to their material abundance and performance. This research first reports the solar cell structure ITO/TiO2/Cu2ZnSn(S,Se)2/HTM/Pt, using elemental Cu, Zn, Sn, and S precursors for the $Cu2ZnSn(S,Se)_2$ absorber layer. The Mo-free CZTS was fabricated using the solution-process method. The analysis of crystallinity, morphology, optics, and electronics of solar cells will be further investigated. (1) The result shows that kesterite crystals have been successfully synthesized based on Cu-poor Cu/(Zn + Sn) = 0.86 and Zn-rich Zn/Sn = 1.25. (2) The crystallinity analysis indicates that the sample had 17.40-31.97% crystallinity. CZTSSe N has the lowest secondary-phase percentage, at 16.2%. (3) The morphological crystal analysis proves that the addition of Se atoms to CZTS L and CZTS N has reduced the grain size from 195.9 to 98.1 nm and 32.8 to 10.7 nm, respectively. (4) The optical analysis shows that the Se atom addition contributes to the absorbance peak redshift and a bandgap decrease of 0.08-0.28 eV. (5) The electronic analysis indicates that the synthesized CZTSSe N is closest to the non-stoichiometric $Cu_{2.1}Zn_{1.25}SnS_2Se_2$ reference, having the slightest error of 16.0%. CZTSSe N exhibits the smallest bandgap of 1.16 eV, contributing to the highest LHE value of 88.12% and the highest efficiency of 0.166%. Interestingly, the local material-based CZTSSe L efficiency is 92%, close to that of CZTSSe N.

Keywords: Solar cell, Kesterite, Non-vacuum fabrication, Element materials

1. Introduction

The B.P. Statistical Review of World Energy in 2019 stated that 85% of the world's current energy needs, totaling 159.200 TWh, come from fossil fuels such as natural gas, coal, and petroleum [1]. Data from the Central Bureau of National Statistics in 2015 revealed that coal accounted for 61.6% of the total energy generated, 161.798 GW, in 2011 – 2015 [2]. This dependence on non-renewable fossil energy continues due to energy needs and is unlikely to impact the depletion of these energy sources [3]. In 2018, it was estimated that the potential for fossil energy from petroleum was around 57×10^{21} J, with consumption of 18×10^{19} J per year [4, 5]. Therefore, it is estimated that it will run out in 316 years. At the same time, the potential for coal-based fossil energy is around 909 billion tons, with consumption increasing by 5% per year. Thus, it is estimated that this energy will last only 155 years [6]. Moreover, environmental and global warming problems arising from CO_2 emissions from fossil fuels worsen the conditions that occur [7]. Therefore, the increasing demand for energy in recent years

and the need to protect the earth from global warming and environmental pollution have heightened enthusiasm for realizing environmentally friendly renewable energy that can meet energy needs.

Solar energy is one of the promising renewable energy sources for the future that could replace fossil fuels [8]. Moreover, converting solar energy through solar cells produces no environmental pollution [3]. The energy transmitted by the sun to the Earth annually is about 5.6×10^{24} joules, equivalent to 10.000 times the world's current energy consumption [9, 10]. As a tropical country, Indonesia has sources of solar energy of up to 4.8 kWh/m^2/day with an area of about 2 million km^2 or about 112.000 GW_P [11]. Based on Presidential Regulation No. 5 of 2006, Indonesia plans to optimize the management of solar energy sources by 5% of the total solar energy demand in 2025 [12]. However, Indonesia's basic solar cell fabrication still heavily relies on supplies from developed countries. Therefore, research into developing solar cells is critical to supporting the independence of Indonesia's solar cell industry.

Solar cells are devices that directly convert solar energy into electrical energy. [13]. Solar cells are made of p-type and n-type semiconductor materials that are connected, allowing charge carriers to diffuse and form a depletion region. [14-16]. Sunlight illuminating solar cells will form electron-hole pairs, which are then separated by an internal electric field in the depletion area. Thus, an electric current is generated [17-19]. This event is called the photoelectric effect, in which there are two types of photons in the broad spectrum of sunlight: photons with energy below the bandgap of solar cell absorbers and photons with energy above it. Photons with less energy will not be absorbed, while photons with greater energy will be absorbed partly into electrical energy and partially into heat energy. Thus, the solar cell absorber absorbs about 45% of the energy from the sunlight spectrum with a bandgap of 1.1 – 1.4 eV [20-22].

Solar cells could be classified into three classes based on their origin. [23]. First, solar cells are made from Si (homojunction and heterojunction), GaAs, and GaInP, which have a very high S-Q efficiency (>75%) [24-26]. Second, multi-crystalline and polycrystalline solar cells with high S-Q efficiency (50-75%), for example, Si, $CuInGa(Se,S)_2$ ("CIGS"), CdTe, methylammonium lead halide perovskite [CH_3NH_3Pd $(I,Cl,Br)_3$], and InP [16, 27-32]. Third, microcrystalline or nanocrystalline and amorphous solar cells with low S-Q efficiency (<50%), such as Si, $Cu_2ZnSn(Se,S)_4$ (CZTS), dye-sensitized TiO_2, organic materials, polymers, and quantum dot materials [10, 18, 19, 33-46]. Research on solar cells made from CZTS as an absorber layer (p-type) has recently become widely discussed [18, 35, 37]. Various studies have been carried out to improve the performance of these solar cells so that they can reach >20% [47]. Compared to previous generations of thin-film solar cells such as CdTe, GaAs, and CIGSe, CZTS-based thin-film solar cells have the advantage of being abundantly available with nontoxic elements [36, 48, 49].

CZTS material is highly suitable for use as an absorbent layer in thin-film solar cells because it closely resembles CIGS [50]. CZTS is a quaternary semiconductor whose atoms are bonded to form a crystal arrangement of the *kesterite* or *stannite* type [51]. Both crystal structures are tetragonal, like CIGS chalcopyrite, but are distinguished by the opposite positions of the Cu and Zn atoms [52]. CZTS-based material is also a p-type semiconductor with a direct band gap (1.0 – 1.5 eV) with an absorption coefficient of 10^4 – 10^5 cm^{-1} [53]. CZTS also has a high hole density of approximately 10^{16} cm^{-3} [54]. Empirically, the composition of the CZTS constituent atoms is generally organized into non-stoichiometric states, Cu-poor and Zn-Rich (fewer Cu atoms than Zn), to produce high efficiency [55-57]. The current world record for the efficiency of CZTS-based thin-film solar cells is 12.6%, achieved through solution-process-based fabrication with CZTS deposition using a spin coater [58]. However, various phenomena that occur in both bulk CZTS and its interfaces, such as recombination and secondary phases, cause the efficiency of CZTS solar cells to remain, in practice, lower than that of CIGS-based solar cells. In addition, the use of molybdenum material (IDR 500.000/piece), which is relatively difficult to find, makes this research necessary to be done to find more effortless sources of material with conductivity capabilities that are almost equivalent to molybdenum, such as Indium Tin Oxide (ITO) (IDR 30.000/piece). The vacuum fabrication and sulfurization process of CZTS, which requires a 3-zone furnace, makes non-vacuum solution-based CZTS fabrication difficult, given the difficulty of achieving a good p-n junction separation that produces the expected open-circuit voltage.

This research contributed to the development of a p-n junction structure in CZTS with a Molybdenum-Free conductive layer via non-vacuum fabrication.

Indonesia has the potential of abundant metal mineral wealth to support the development of the solar cell industry (especially in West Java), such as 10.3 tons of gold (Au), 28.44 tons of silver (Ag), 221.2-kilo tons of Zinc (Zn), 14.4-kilo tons of copper (Cu), 60-kilo tons of tin (Sn), 2.7 million tons of Titanium (Ti) [59, 60]. To support Law No. 4 of 2009 in place of Law No. 11 of 1967 as an effort to develop third-generation solar cells [61]. Thin-film solar cells based on CZTS are believed to have the potential to become the future solar cells that can replace conventional silicon-based solar cells. The availability of abundant materials for CZTS, which can reduce dependence on rare materials such as In, Ga, and As, and on toxic materials such as CdTe, is an important reason to pursue continuous development. Therefore, intensive research is needed to increase its efficiency to> 20% so it can be commercialized. The research utilized local materials Cu, Zn, Sn, and S as the main precursors for Cu_2ZnSnS_4 and $Cu_2ZnSn(Se,S)_2$ absorber layers. These two materials were chosen because the CZTS and CZTSSe have a band gap of about 1.0-1.5 eV. Thus, the research results can inform the development of independent and competitive techniques for depositing Mo-free CZTS via a solution-process method on TiO_2/ITO films. Considering that the TiO_2/ITO layer has been analyzed comprehensively in several previous studies [38, 41, 43, 62, 63]The use of toxic material Cadmium (CdS) as a standard n-type buffer layer in the CZTS cell structure will be replaced with Hole-Transport-Material, which has been optimized in previous studies [39]. Therefore, the novelty of this research is the use of locally sourced, element-based Mo-free CZTS with a buffer layer of a Cd-free hole-transport material, forming a complete structure of ITO/TiO_2/Cu2ZnSn(S, Se)$_2$/HTM/Pt. Optical and electronic characterization will be performed to analyze the performance of $Cu_2ZnSn(S, Se)_2$ solar cells. The percentages of Cu2ZnSnS4 and Cu2ZnSnSe4 crystals in the absorber layer were also analyzed using the reference intensity ratio (RiR) method.

2. Experiment Method

2.1. Materials

This research method is divided into two stages: cell fabrication and characterization. The experiment used local element material precursor powders: Cu, Zn, Sn, and S 99.9% as test parameters, as shown in Fig 1. Precursors of $Cu(CH_3CO_2)_2 \cdot H_2O$, $Zn(CH_3CO_2)_2 \cdot 2H_2O$, $SnCl_2 \cdot 2H_2O$, $SC(NH_2)_2$, and Se from Merck were used as standard materials as tabulated in Table 1. Indium Tin Oxide (ITO–sheet resistance 6 Ω/sq) conductive transparent film, TiO_2 nanomaterial, I^-/I_3^- based hole transport material containing Iodine/Lithium iodide/1-butyl-3-methylimidazolium-iodide/4-tert-butyl-pyridine/Acetonitrile/Polyethylene-oxide, counter electrode Pt Platinum used as the control parameter.



Figure 1. Local Element Powder Materials (Cu, Zn, Sn, and S – *from left to right*)

Table 1. Sample composition for CZTS synthesis

No	CZTS L	CZTS N	Molarity (mmol)
1	Cu	$Cu(CH_3CO_2)_2 \cdot H_2O$	15,3
2	Zn	$Zn(CH_3CO_2)_2 \cdot 2H_2O$	10
3	Sn	$SnCl_2 \cdot 2H_2O$	8
4	S	$SC(NH_2)_2$	32

No	CZTS L	CZTS N	Molarity (mmol)
No	**CZTSSe L**	**CZTSSe N**	**Molarity (mmol)**
1	Cu	$Cu(CH_3CO_2)_2 \cdot H_2O$	15,3
2	Zn	$Zn(CH_3CO_2)_2 \cdot 2H_2O$	10
3	Sn	$SnCl_2 \cdot 2H_2O$	8
4	S	$SC(NH_2)_2$	16
5	Se	Se	16

This study used four samples, namely CZTS L, CZTS N, CZTSSe L, and CZTSSe N, as shown in Table 1. First, the CZTS absorber solution was made with the four samples. Second, it was fabricated using the sol-gel method. Third, a standard TiO_2 paste and an I-/I3- electrolyte were prepared. Fourth, the samples were deposited using a spin-coating technique. Then, the sample was sandwiched between the working electrode $TiO_2/Cu_2ZnSn(S, Se)_2$ and the reverse electrode Pt by inserting it between the transport holes of the solid electrolyte-based material I^- and I_3^-.

2.2. Kesterite Absorber Layer Synthesis

The fabrication of kesterite absorber layers began with the preparation of tools and materials, as shown in Table S1. The synthesis was performed by dissolving all the ingredients in 2-methoxyethanol, then heating at 50 °C for 2 hours. Afterward, the solution was left for 12 hours and filtered. A few drops of trimethylamine (TMA) and monoethylamine (MEA) were added to the CZTS precursor solution. The absorber layer was deposited on an ITO glass substrate by spin-coating and preheated at 170 °C for 2 minutes. Spin coating and preheating were repeated to gain the expected thickness. Next, the sample was heated at 500 °C for 30 minutes at a heating rate of 2 °C/minute, then cooled to room temperature.

2.3. Standard TiO_2 Synthesis

The fabrication of TiO_2 films was carried out utilizing a sol-gel approach. Initially, the base solvent was prepared by combining equal volumes (30 mL each) of water and acetic acid, which was then agitated at 600 rpm for 5 minutes. To inhibit particle agglomeration, 1.5 g of polyethylene glycol (PEG, MW = 20,000) alongside 5 g of P25 TiO_2 powder were introduced into the mixture, followed by continuous stirring at 600 rpm for 3 hours. Subsequently, a few drops of Triton-X100 were incorporated, and hydrochloric acid was gradually added to adjust the acidity to pH 1.0. This acidification is a crucial step to stabilize the nanoparticles and promote anatase phase crystallization. The suspension was then heated to a steady 80 °C under constant 600 rpm stirring, followed by a 3-hour ultrasonication treatment to produce a highly homogeneous TiO_2 paste. For the deposition phase, the resulting paste was spin-coated at 4000 rpm for 30 seconds onto Indium Tin Oxide (ITO) glass substrates (dimensions: 2 × 2.5 cm², active frame: 0.5 × 0.5 cm²). This coating cycle was repeated until ted a target thickness of 10.58 µm. Ultimately, the samples underwent a sequential, three-stage annealing process at a heating rate of 2 °C/min: 125 °C for 15 minutes, 325 °C for 15 minutes, and concluding at 450 °C for 30 minutes [9,10].

2.4. Hole Transport Material Preparation

To formulate the liquid electrolyte, 0.1 M lithium iodide (LiI) and 0.05 M iodine (I_2) were first dissolved in 100 mL of acetonitrile. This initial mixture was agitated at 300 rpm for 5 minutes to ensure complete homogeneity. Subsequently, 0.6 M 1-butyl-3-methylimidazolium iodide (BMII) and 0.5 M 4-tert-butylpyridine (TBP) were incorporated into the solution, which was then subjected to continuous mechanical stirring overnight [9,10]. The resulting I^-/I_3^- redox electrolyte was transferred to an amber glass vial and stored at ambient room temperature before its application.

2.5. Preparing $TiO_2/Cu_2ZnSn(S,Se)_2$ Solar Cells

First, the synthesized standard TiO_2 was deposited onto the ITO glass and heated in three steps, as mentioned in the previous standard TiO_2 synthesis. Second, a CZTS absorber layer was added and

heated at 500°C for 30 minutes. Next, the quasi-solid-state electrolyte was added to the TiO_2/CZTS film. Then, the TiO_2/CZTS film layer was covered with Pt/ITO glass 2 × 2.5 cm^2 in size.

2.6. Materials Characterizations

Characterizing the crystal structure using X-ray diffraction (XRD) was intended to determine the crystal phase formed in the CZTS absorber layer and the number of phases present. A Bruker Advanced D8 instrument assisted the characterization with Cu-Kα excitation. Based on the diffraction pattern obtained, the XRD characterization results were processed using Match! Phase Analysis used Powder Diffraction 3.3 to determine the percentage of each phase formed in both the kesterite and secondary phases using the reference intensity ratio (RiR) method.

Microstructural analysis by Scanning Electron Microscope (SEM) was conducted to examine the absorber layer and the cross-section of the CZTS solar cell. The SEM test equipment is the HitachiTM SU-3500. UV-Vis spectroscopy is used to characterize the optical properties of the CZTS absorber layer. This characterization could determine the optical properties (Absorption, Transmittance) and the Bandgap (Eg). The UV-Vis spectrometer was equipped with a computer for data analysis. Characterization of UV-Vis spectra was performed using a UV-Vis Spectrophotometer 1600PC. The J-V characteristics of solar cells were needed to find out the photocurrent density (J_{sc}), the open circuit voltage (V_{oc}), the fill factor (FF), and the efficiency (η) of the solar cells using a 200W LED Solar Simulator Lamp filtered with AM 1.5 100 mW/cm^2. An ADCMT6342 digital multimeter recorded current and voltage.

3. Results and Discussion

3.1. Solar Cell Fabrication Analysis

Synthesis of CZTS precursors used the solution-process method, with precursors as previously described in Table 1. In addition, the non-stoichiometric CZTS absorber layer synthesis based on Cu-poor Cu/(Zn+Sn) = 0.86 and Zn-rich Zn/Sn = 1.25 was used as the basis for calculating the precursor ratio [64-66]. Figure 2 shows the synthesis results of CZTS L and CZTSSe L made from local element materials and CZTS N and CZTSSe N made from standard materials.



Figure 2. Synthesized local and standard CZTS precursors

The synthesized solutions of CZTS and CZTSSe made locally are orange, whereas those made from standard sources are light blue and dark blue-black. The results of synthesized CZTS and CZTSSe on the TiO_2/ITO films are shown in Figure 3. TiO_2/$Cu_2ZnSn(S, Se)_2$ solar cells were fabricated by adding material transport holes and covered with Pt/ITO reverse electrodes, as illustrated in Figure 4.

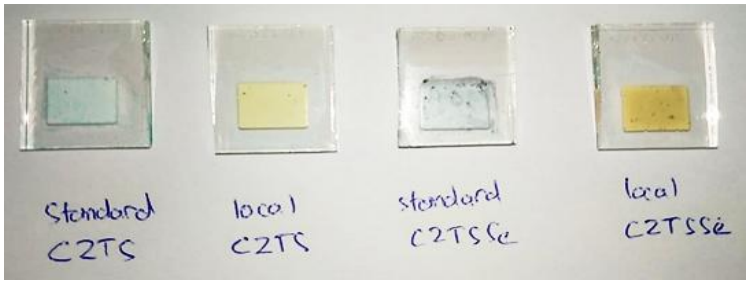


Figure 3. CZTS N, CZTS L, CZTSSe N, and CZTSSe L thin films (left to right)

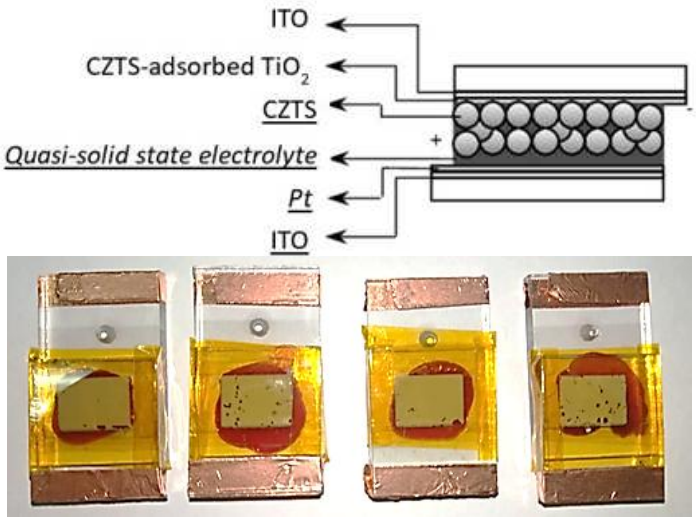


Figure 4. CZTS solar cell design (top) and $TiO_2/Cu_2ZnSn(S,Se)_2$ solar cell fabrication (bottom)

3.2 Crystallinity Analysis

The crystal structures of the samples were characterized by X-ray Diffraction (XRD), as presented in Figure 5. XRD characterization was carried out to analyze the structure of $Cu2ZnSn(S, Se)_2$ formed after calcination, secondary phase, crystallinity, non-stoichiometric ratios of Cu/Zn+Sn, Zn/Sn, and S/Se post-synthesis, as well as grain size based on full-width at half maximum (FWHM) data of the kesterite diffraction peak. In addition, x-ray diffraction pattern analysis of the film semiconductors was conducted using the reference intensity ratio (RiR) method with Match!. Phase Analysis using Powder Diffraction software version 3.3. The results of the analysis are also presented in Figure 6.

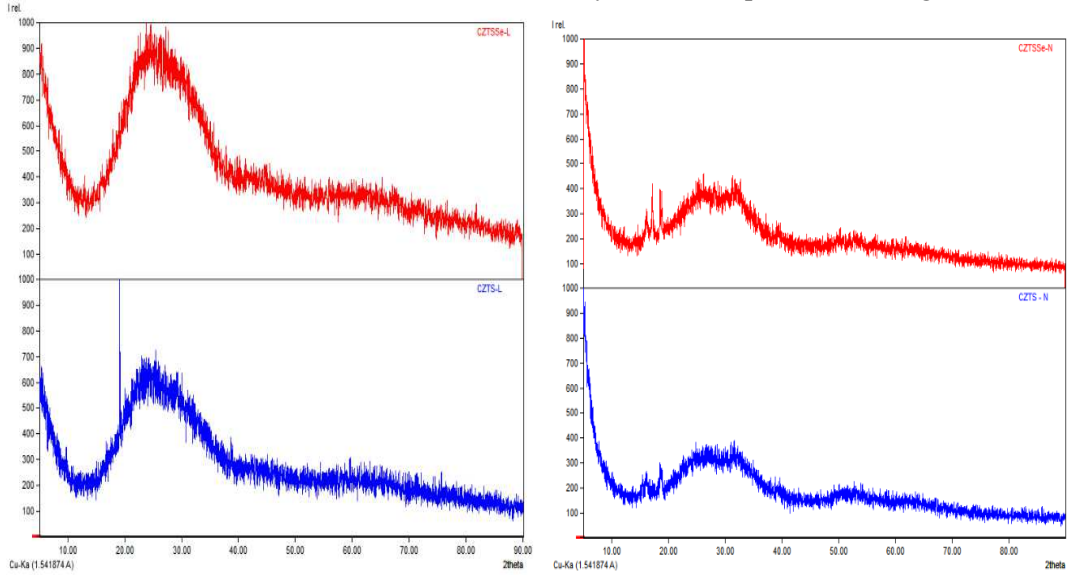


Figure 5. X-ray diffraction patterns of CZTS-L, CZTS-N, CZTSSe-L, and CZTSSe-N kesterite semiconductors

Based on XRD analysis, the secondary phases observed were Cu_2S, Cu_2Se, Cu_2SnS_3, Cu_2SnSe_3, ZnS, ZnSe, SnS, SnSe, SnS_2, $SnSe_2$. The secondary phase was observed by comparing the reference diffraction pattern taken from each secondary Phase's Crystallography Open Database (COD). Table S2 describes the reference standards used for crystal analysis. $TiO_2/Cu_2ZnSn(S, Se)_2$ solar cells were fabricated by adding material transport holes and covered with Pt/ITO reverse electrodes, as illustrated in Figure 4.3. Crystal analysis employed the reference intensity ratio (RiR) method, which uses a COD

reference to analyze secondary phases formed in the absorber layer. The graph in Figure 6 shows the peaks corresponding to the secondary phases formed in the absorber layer.

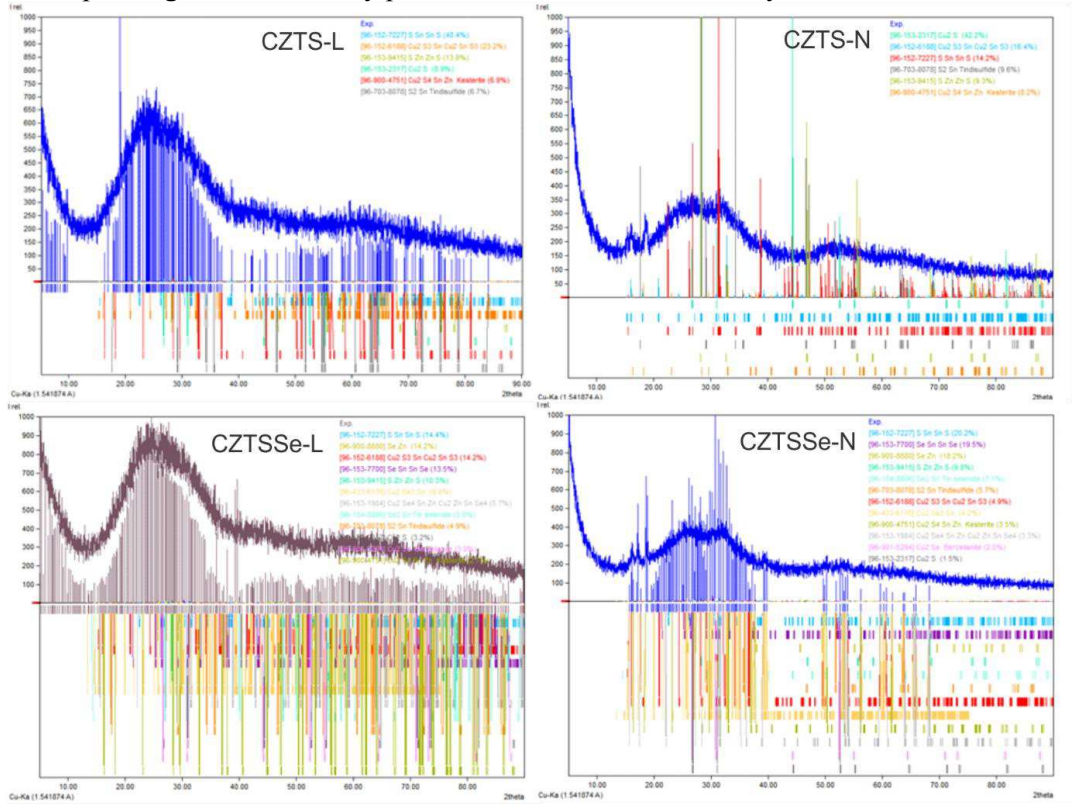


Figure 6. X-ray diffraction pattern analysis of CZTS-L, CZTS-N, CZTSSe-L, and CZTSSe-N semiconductors using the reference intensity ratio (RiR) method

Table 2. Kesterite crystals analysis by the reference intensity ratio (RiR) method

Sample	Elementary Ratio	Crystallinity (%)	Secondary Phase (%)	Amorphous (%)
CZTS L	$Cu_{1.8}ZnSn_{2.3}S_5$	25.31	23.54	74.69
CZTS N	$Cu_{3.4}ZnSn_{3.1}S_{6.9}$	21.99	20.16	78.01
CZTSSe L	$CuZnSn_{1.3}S_{1.9}Se_{1.4}$	31.97	29.32	68.03
CZTSSe N	$Cu_{0.5}ZnSn_{1.4}S_{1.6}Se_{1.4}$	17.40	16.20	82.60
Reference	$Cu_{2.1}Zn_{1.25}SnS_2Se_2$	100.00	0.00	0.00

Table 2 revealed that all the samples made have crystallinities between 17.40 and 31.97%. CZTSSe L produced the best crystallinity of 31.97%, while CZTSSe N produced the lowest crystallinity of 17.40%. This result occurs because the CZTS crystals, which should have formed in the kesterite phase, did not fully form. Based on previous studies, higher-concentration CZTS structures can be obtained by sulfurization in an $N_2 + H_2S$ gas atmosphere, resulting in higher, sharper diffraction peaks compared to the room atmosphere. [67]. Based on this result, the 68.0-82.6% amorphous content in the absorber layer observed in this experiment was due to the lack of H_2S sulfurization. Therefore, the absorber layer results in a more amorphous formation than crystals. It can also be seen that the peaks in the sample are not as sharp as those in the reference.

Table 3. The percentage of kesterite crystals in the absorber layer was analyzed based on the reference intensity ratio (RiR) method

Sample	Cu_2ZnSnS_4 (%)	$Cu_2ZnSnSe_4$ (%)	Cu/Zn+Sn	Zn/Sn	S/Se	% error
CZTS L	1.75	-	0.55	0.43	-	66.0
CZTS N	1.80	-	0.84	0.32	-	74.3
CZTSSe L	0.86	1.82	0.44	0.77	1.37	37.8
CZTSSe N	0.61	0.57	0.20	0.74	1.15	16.0
Reference	50.00	50.00	0.85	1.25	1	0

The results indicated that the CZTSSe N elemental ratio has a minor error and is closest to the expected non-stoichiometric reference ratio, with a standard error of 16.0%, as shown in Table 3. In addition, CZTSSe N has the lowest secondary phase percentage (16.2%) among the samples. On the other hand, the presence of selenium atoms in CZTS crystals can bind Cu_2ZnSn atoms better than sulfur atoms. Consequently, they have a minor error (16.0-37.8%) than the CZTS structure (66.0-74.3%).

Table 4. Analysis of the secondary phase of the formation of kesterite crystals

Sample	Cu_2S (%)	Cu_2Se (%)	Cu_2SnS_3 (%)	Cu_2SnSe_3 (%)	ZnS (%)	ZnSe (%)	SnS (%)	SnSe (%)	SnS_2 (%)	$SnSe_2$ (%)
CZTS L	2.25	-	5.87	-	3.49	-	10.23	-	1.70	-
CZTS N	9.28	-	3.61	-	2.05	-	3.12	-	2.11	-
CZTSSe L	1.02	0.96	4.54	2.88	3.29	4.54	4.60	4.32	1.57	1.60
CZTSSe N	0.26	0.35	0.85	0.73	1.71	3.17	3.51	3.39	0.99	1.24

Table 4 presents the secondary-phase analysis of Cu_2S, Cu_2Se, Cu_2SnS_3, Cu_2SnSe_3, ZnS, ZnSe, SnS, SnSe, SnS_2, and $SnSe_2$ in the absorber layer. First, the mass percentage of each secondary Phase formed in the absorber layer was determined using the reference intensity ratio (RIR) method. Next, the percentage of secondary-phase crystals was analyzed by comparing the mass percentage with the relative molecular mass and the total crystallinity in the absorber film. Based on the analysis, it was known that CZTS produces a secondary phase of $Cu_2(S/Se)$, which is more dominant than CZTSSe. The results indicated that Se atoms could bind Cu more strongly, producing a kesterite structure with higher crystallinity than S atoms. The higher Cu elemental ratio values also reinforced this in CZTS compared to CZTSSe, as shown in Table 3. Consequently, CZTS produces a lower fill factor (46.3-49.0%) than CZTSSe (49.8-50.5), as presented in Table 9.

Table 9. Solar cells performance

Devices	E_g (eV)	E_g-V_{oc} (V)	LHE (%)	J_{sc} (mA.cm^{-2})	V_{oc} (V)	FF (%)	η (%)
TiO_2/CZTS L/HTM/Pt	3.26/1.54	1.24	80.42	0.972	0.300	46.3	0.135
TiO_2/CZTS N/HTM/Pt	3.26/1.44	1.05	87.64	0.806	0.390	49.0	0.154
TiO_2/CZTSSe L/HTM/Pt	3.26/1.46	1.12	84.49	0.901	0.340	49.8	0.153
TiO_2/CZTSSe N/HTM/Pt	3.26/1.16	0.74	88.12	0.782	0.420	50.5	0.166
TiO_2/HTM/Pt	3.26	2.88	16.44	0.560	0.380	47.7	0.102

Local element materials produced higher $Cu_2Sn(S/Se)_3$ and Sn(S/Se) secondary phases than standard materials. This finding is due to the absence of dissolved Zn atoms during synthesis, which made it easier for Cu-Zn-S/Se to form a secondary phase. In subsequent studies, the order of powder mixing and several parameters, such as reaction temperature and the length of the synthesis process, need to be re-examined to improve the synthesis results and reduce the secondary Phase. [68, 69]. This data was supported by the invisible absorption peak at 705-713 nm in the local kesterite material, as observed in the standard kesterite material. Consequently, local materials in solution and crystalline states after deposition on TiO_2 resulted in lower light-harvesting efficiency values (80.42-84.49%) than standard materials (87.64-88.12%). Therefore, the surfactants could be In addition, the content of the secondary phase $Cu_2Sn(S/Se)_3$ and Sn(S/Se) would have an impact on reducing the efficiency of the kesterite solar cell because the secondary phase interface will cause an increase in the recombination rate where the secondary Phase has a bandgap close to the kesterite. [70-73]. Furthermore, upon formation of the secondary phase, the electric field will inhibit electron transfer across the p-n junction. [72].

The total secondary Phase and distribution for each sample are easier to read in Figure 7. The net diagram of the secondary phase in the kesterite semiconductor showed that a smaller area indicated lower secondary-phase content in the sample. Based on Figure 7, CZTSSe N has the smallest area, indicating the lowest secondary phase content.

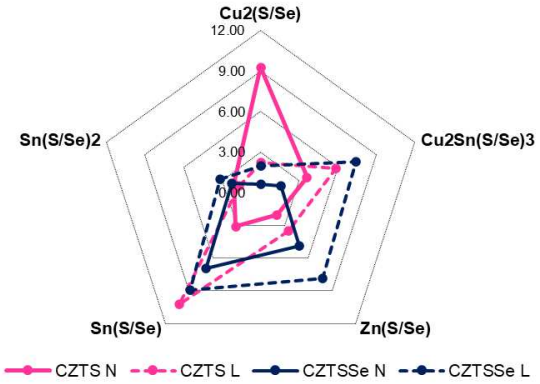


Figure 7. The net diagram of the secondary Phase of the kesterite semiconductor based on the analysis of the X-ray diffraction pattern of the semiconductor using the reference intensity ratio (RiR) method

CZTSSe produced higher Zn(S/Se) and $Sn(S/Se)_2$ secondary phases than CZTS. It was easier for Se atoms to bind Zn atoms than S atoms to Zn atoms, as described in Table 4, wherein CZTSSe L, ZnSe formed was 4.54% compared to ZnS formed at 3.29%. In CZTSSe N, the ZnSe formed was 3.17%, compared to 1.71% for ZnS. In addition, Se atoms are also easier to bind to Sn than S atoms bind to Sn. In CZTSSe L, the $SnSe_2$ formed was 1.60%, compared to 1.57% for SnS2. Likewise, in CZTSSe N, the $SnSe_2$ formed was 1.24%, compared to 0.99% for SnS_2. The formation of an electric field by the secondary phases Zn(S/Se) and Sn(S/Se)2 will inhibit the electron-transfer rate. Thus, it was proven that CZTSSe produces a lower electric current (0.024-0.071 mA/cm^2) than CZTS. Reducing the secondary phase in Zn(S/Se), which is more dominant than in Sn(S/Se)2, is key to increasing electron transfer in kesterite solar cells. This evidence supports the previous findings of Refantero et al. [35] and Ashfaq et al.[70], Liu et al. [74] et Mendis et al. [72].

3.3 Kesterite Crystalline Morphological Analysis

The morphological characteristics of kesterite crystals were tested using a Scanning Electron Microscope (SEM). Using this method, the surface microstructure of the CZTS absorber layer could be analyzed and corroborated by grain-size data from FWHM analysis of XRD data. The surface microstructure of the absorber layer of each sample is shown in Figure 4.7. To measure the mean grain size of the material from the XRD diffraction pattern, the Full Width at Half-Maximum height (FWHM) data was processed using the Debye Scherrer formula [75, 76], as shown in Eq. 1.

$$\boldsymbol{D = \frac{K\lambda}{\beta cos\theta}} \quad (1)$$

Where λ is the X-ray wavelength used during the test, which is 1.54187 A, K is a constant with a value of 0.9, β is FWHM, and D is the average grain size formed on the absorber layer. The average grain size of the absorber layer for each sample was presented in Table 5.

Table 5. Grain size analysis of kesterite crystals based on XRD diffraction patterns

Sample	θ (rad)	FWHM	d (nm)
CZTS L	0.143	0.00072	195.9
CZTS N	0.162	0.00429	32.8
CZTSSe L	0.144	0.00143	98.1
CZTSSe N	0.143	0.01311	10.7

Figure 8 shows the surface morphology of the CZTS absorber thin film for the four samples, CZTS-L, CZTS-N, CZTSSe-L, and CZTSSe-N. It could be assumed that the CZTS L sample has a uniform shape with CZTSSe L in sheet form. At the same time, CZTS N has a uniform shape, whereas CZTSSe N is

round and smaller than the local materials. These findings supported the grain-size analysis based on the XRD results in Table 5.

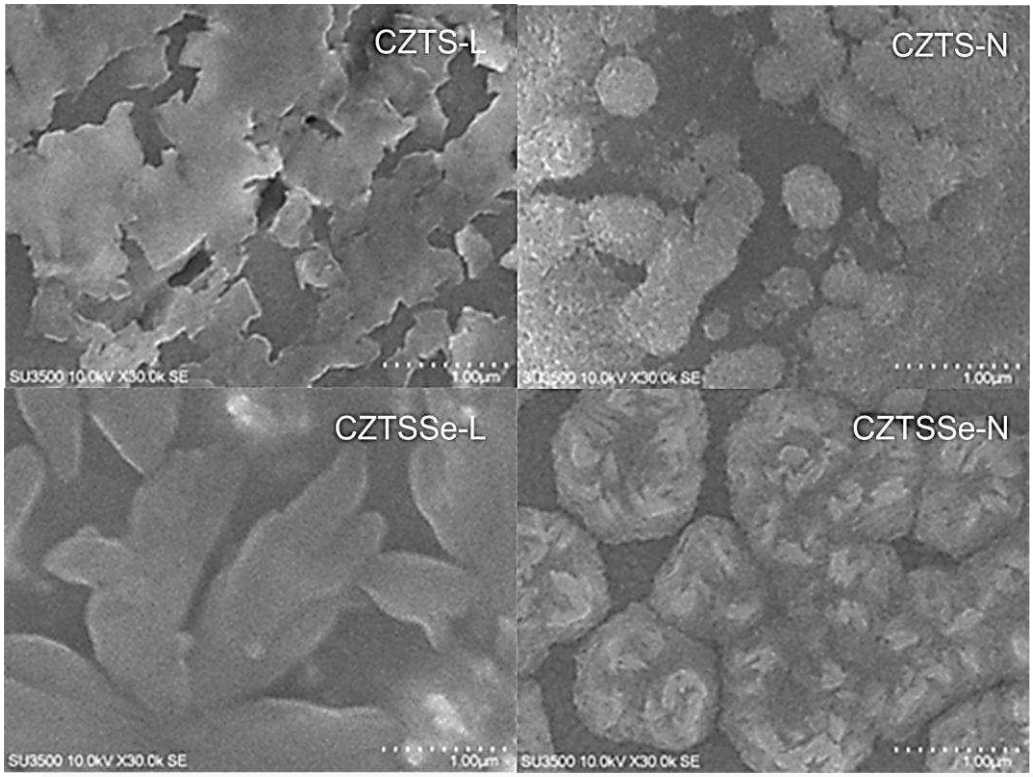


Figure 8. Scanning electron microscope (SEM) photo of the crystalline film surface (a) CZTS-L, (b) CZTS-N, (c) CZTSSe-L, (d) CZTSSe-N with 30,000 times magnification

Further investigation indicated that the addition of Se atoms to CZTS led to a 2-3-fold decrease in grain size in both local and standard materials. For example, the grain size of CZTS-L, whose original size was 195.9 nm, became 98.1 nm after adding Se atoms in CZTSSe-L. While the grain size of CZTS-N, whose original size was 32.8 nm, became 10.7 nm after the addition of Se atoms in CZTSSe L. With a smaller grain size, the crystals will be more readily adsorbed on the porous surface of TiO_2. As a result, they could increase the amount of kesterite adsorption on the TiO_2 film.

Table 2 presents the decrease in Cu concentration according to elemental ratio analysis: from Cu1.8 to Cu1.0 in CZTS L and from Cu3.4 to Cu0.5 in CZTS N in CZTSSe. The decrease in crystal size has been previously studied by Kumar et al. [77], where the decrease in Cu concentration in the crystals contributes to a decrease in grain size. Bhosale et al. [78] Also found that grain size increased with increasing Cu concentration in CZTS.

The entire sample is also porous, allowing it to be well adsorbed onto the TiO2 layer, forming a p-n junction. The absorber layer's pore formation would reduce the film's reflectance, thereby increasing the amount of light absorbed. It would help reduce the bandgap and improve light-harvesting efficiency. Porus, in this case, would provide a quantum confinement effect, thereby reducing electron-hole recombination and increasing solar cell efficiency. The data in Table 8 indicates that the bandgap CZTSSe L (1.46 eV) < CZTS L (1.54 eV), and also the bandgap CZTSSe N (1.16 eV) < CZTS N (1.44 eV). The data in Table 7 also show that light-harvesting efficiency (LHE) of CZTSSe L (84.49%) > CZTS L (80.42%), and LHE of CZTSSe N (88.12%) < CZTS N (87.64%).

3.4. Kesterite Solar Cells Optical Properties

The optical characteristics of the kesterite absorber layer were analyzed using UV-Vis spectroscopy. Figure 9 reports the absorption of UV-Vis light of CZTS N, CZTS L, CZTSSe N, and CZTSSe L post-synthetic samples before calcination.

Table 6. Uv-Vis absorbance analysis

Sample	λ_1 (nm)	A_1 (a.u.)	λ_2 (nm)	A_2 (a.u.)
CZTS L	300	2,19	418	0,32
CZTS N	306	3,91	705	0,85
CZTSSe L	302	2,56	423	0,34
CZTSSe N	308	4,25	713	1,06

Based on the analysis of UV-Vis absorption peaks in Table 6, the CZTS synthesis solution has the main peak at 300-308 nm, the second peak for local materials at 418-423 nm, and the standard material at 705-713 nm. The first peak contributed to the absorber film's maximum light-harvesting efficiency, which ranged from 99.8% to 99.9%, as shown in Table 4. This finding was in line with the research of Refantero et al. [35] and Katagiri et al. [79, 80]. Another promising finding was that the addition of Se atoms contributed to the redshift of each peak, which decreased the bandgap by 0.08-0.28 eV, as shown in Table 8. CZTSSe N in this study exhibited high light absorption because its smallest particle size (10.7 nm) facilitated greater absorption, and the smallest total secondary Phase compared to other crystals (16.20%). Based on Table 4, it can also be inferred that the standard material exhibited a red shift towards local materials because the salt precursor bonds used were more readily dissolved in the solvent 2-methoxyethanol than in Cu, Zn, Sn, and S powders.

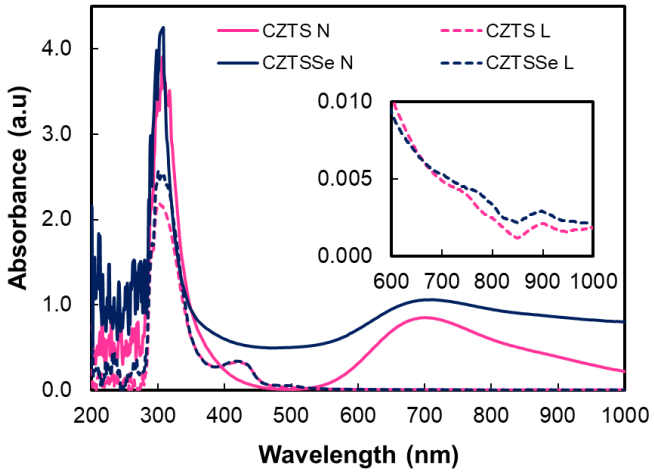


Figure 9. UV-Vis absorption spectrum of the synthesized kesterite solutions CZTS N, CZTS L, CZTSSe N, and CZTSSe L before calcination

In addition, analysis of absorbance data and light-harvesting efficiency was carried out by plotting absorbance versus wavelength and percentage of LHE. Light-harvesting efficiency (LHE) is defined as the fraction of the incident light intensity absorbed by the crystal at a specific wavelength. [81]. The percentage of LHE is calculated in Eq. 2.

$$\boldsymbol{LHE}\,(\%) = (\mathbf{1} - \mathbf{10}^{-\alpha}) \times \mathbf{100}\% \qquad (2)$$

The LHE graph is shown in Figure 10.

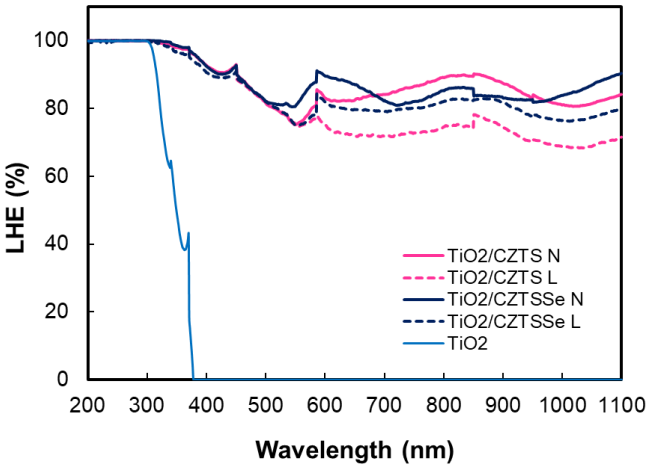


Figure 10. Light harvesting efficiency of solar cells CZTS N, CZTS L, CZTSSe N, CZTSSe L, TiO_2

Figure 10 shows that, after sulfurization, the four kesterite samples have similar LHE spectral patterns across all absorption peaks compared to TiO_2. The three-wave peaks at 450, 586, and 851 nm of the solution-processed kesterite sample are shown in Figure 9. This result indicated that the four samples formed a kesterite structure with compositional details described in the previous crystallinity analysis. The kesterite structure broadens the absorption range from a maximum at 381 nm in TiO2 to 1069 nm, thereby increasing light-absorption efficiency by up to 71.68%.

Table 7. Data analysis of light harvesting efficiency and absorption peaks of solar cells

Sample	$\boldsymbol{LHE_{peak_1}}$ **(%)**	$\boldsymbol{LHE_{peak_2}}$ **(%)**	$\boldsymbol{LHE_{peak_3}}$ (%)	$\boldsymbol{LHE_{max}}$ **(%)**	$\boldsymbol{\overline{LHE}_{200-1100}}$ **(%)**
TiO_2/CZTS L	**92.82**$_{450nm}$	77.74$_{586nm}$	78.10$_{851nm}$	99.94$_{234nm}$	80.42
TiO_2/CZTS N	**92.82**$_{450nm}$	85.43$_{586nm}$	**90.08**$_{851nm}$	99.94$_{234\ nm}$	87.64
TiO_2/CZTSSe L	90.90$_{450nm}$	84.23$_{586nm}$	82.50$_{851nm}$	**99.95**$_{244nm}$	84.49
TiO_2/CZTSSe N	92.59$_{450nm}$	**91.01**$_{586nm}$	85.82$_{850nm}$	99.85$_{249nm}$	**88.12**
TiO_2	0	0	0	99.79$_{213nm}$	16.44

The data in Table 7 showed that using Se material in CZTS did not shift the absorption peak of the CZTS absorber layer but managed to increase the average efficiency of light absorption by 0.49-4.07%. TiO_2/CZTSSe N layer produced the highest $LHE_{(200-1100)}$ value of 88.12%. The presence of the secondary phase content of $Cu_2Sn(S/Se)_3$ and Sn(S/Se) in the local material, which was higher than the content of the secondary phase in the standard material, causes the average LHE of the local material to be lower than that of the standard material. The smaller particle size of CZTSSe, compared with CZTS, also contributes to improved light-harvesting efficiency. According to this analysis, locally made Cu-Zn-Sn-S materials with insignificant differences in optical characteristics offer strong potential for developing low-cost, high-performance solar cells in subsequent studies. The main challenges are to reduce the concentrations of the secondary $Cu2Sn(S/Se)_3$ and Sn(S/Se) phases during the formation of kesterite crystals and to increase Cu-Zn-Sn-S bonding in research on the development of locally sourced, material-based kesterite materials.

3.5. Kesterite Solar Cells Performance Analysis

The band gap is determined using Tauc's Plot Method, estimated by Eq. 3 [82, 83].

$$\boldsymbol{\alpha h\nu \approx \left(h\nu - E_g\right)^{\frac{1}{n}}} \quad (3)$$

The band gap is determined by e, alpha = 0. E.g., the bandgap value is related to the light absorption value, and *hv* is the photon energy. Where n = ½ for allowed direct transitions, n = $\frac{3}{2}$ for forbidden direct transitions, n = 2 for allowed indirect transitions, and n = 3 for forbidden indirect transitions. Considering that CZTS is a material with a direct allowed bandgap, the bandgap of this material is

determined using ½ [84]. UV-Vis spectroscopy data were analyzed to determine the bandgap of the kesterite semiconductor using Tauc's Plot method, as described in Eq. 3.

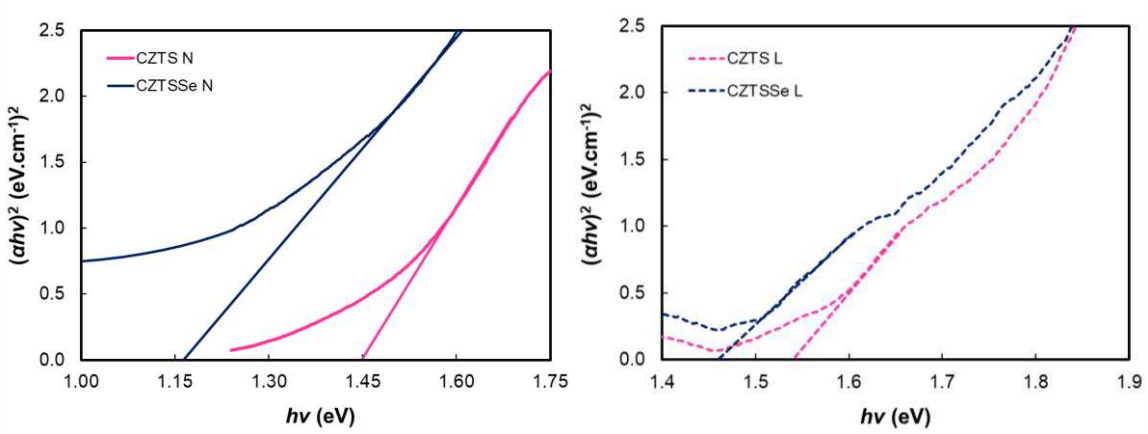


Figure 11. Graph of direct bandgap analysis of CZTS N, CZTS L, CZTSSe N, and CZTSSe L crystals based on Tauc's plot analysis

Table 8. Direct bandgap data of kesterite crystal films based on Tauc plot analysis and their relationship to LHE and solar cell efficiency

Sample	Eg (eV)	d (nm)	$\overline{LHE}_{200-1100}$ (%)	η (%)
CZTS L	1.54	195.9	80.42	0.135
CZTS N	1.44	32.8	87.64	0.154
CZTSSe L	1.46	98.1	84.49	0.153
CZTSSe N	1.16	10.7	88.12	0.166

Figure 11 reports Tauc's curve to determine the bandgap of the four kesterite samples. Table 8 relates the bandgap trend to the morphological properties of grain size. Based on the data, it could be concluded that the smaller the kesterite grain size, the smaller the kesterite bandgap. This result is due to the content of the secondary phases, Cu2Sn(S/Se)3 and Sn(S/Se), in the local material, which affects the large grain size in CZTS L and CZTSSe L. In addition, forming pores in the absorber layer with a small grain size will reduce the film's reflectance. Consequently, the absorbed light could increase due to the presence of pores. Therefore, CZTSSe N, with the smallest bandgap, contributed the most significant LHE (88.12%) among the samples. As a result, CZTSSe N achieved the highest efficiency among the samples. On the other hand, the efficiency of CZTSSe L was 92%, close to that of CZTSSe N.

The overall efficiency of the DSSC (η) is determined by the short-circuit density (J_{sc}), open-circuit voltage (Voc), cell fill factor (FF), and incident light intensity (Is), as described in the following Eq. (4).

$$\eta = \frac{J_{sc} \cdot V_{oc} \cdot ff}{I_s} \tag{4}$$

The other parameter that affects DSSC efficiency is the fill factor (FF), as shown in Eq. (4). This parameter quantifies how well the system operates. The light absorption efficiency, the number of electrons generated and flowing out of the film, is represented by the value of FF.

$$FF = \frac{V_{max} \cdot J_{max}}{V_{oc} \cdot J_{sc}} \tag{5}$$

Figure 12 demonstrates the I-V characteristic curves for the six samples. The graph indicated that the TiO_2/CZTS L solar cells produced the highest *Jsc* (0.972 mA.cm^{-2}), and the low secondary Phase of Cu_2S and ZnS contributed to the high LHE value at the first peak, thereby reducing recombination and increasing the sample Jsc. TiO_2/CZTSSe N solar cells achieved the highest Voc and F.F. (0.42 V and

50.5%, respectively). The low energy gap and the small size supported this data. In addition, CZTSSe N has a minor error or is closest to the non-stoichiometric ratio of the expected $Cu_{2.1}Zn_{1.25}SnS_2Se_2$ reference with a standard error of 16.0% [85, 86]. CZTSSe N also has the lowest secondary phase percentage (16.2%) among the samples, thereby contributing to the high Voc and electrical contact. Compared to TiO_2 cells alone, adding a kesterite structure could increase the maximum performance of TiO_2 solar cells by up to 63%. The high potential for E_g-V_{oc} drop in local materials poses a challenge in reducing the secondary Phase during the synthesis and calcination of kesterite.

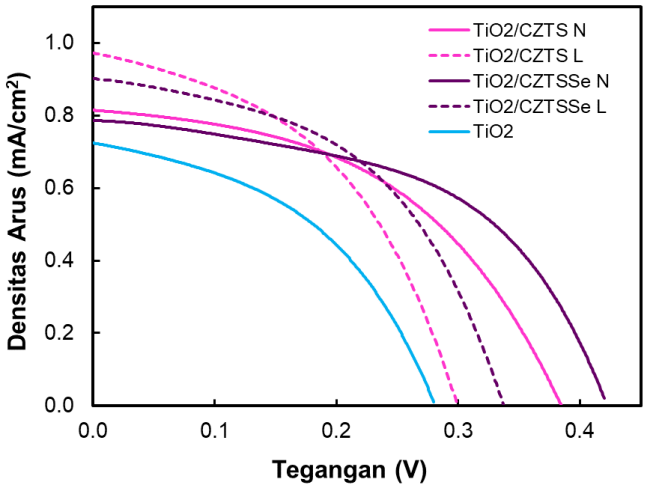


Figure 12. I-V characteristics of CZTS N, CZTS L, CZTSSe N, CZTSSe L, and TiO_2 solar cells

Several factors became limitations in the experimental activities conducted. One of them was the absence of a vacuum tube during the sulfurization process in an H2S environment, which led to high amorphous production. Thus, it is not easy to get better efficiency. The effect of sulfurization is very significant since sulfur atoms are needed to completely bind Cu-Zn-Sn atoms and reduce the formation of the secondary Phase. The unavailability of a sputtering device to deposit the ITO conductive layer above the buffer layer was resolved by adding material transport holes, enabling the solar cell fabrication process to proceed without sputtering. As a result, the solar cell structure ITO/TiO2/Cu2ZnSn(S, Se)^2/HTM/Pt is the first reported in this study. Hence, the development of locally made materials significantly contributes to the development of low-cost, silicon-free solar cells without sputtering.

4. Conclusion

The results of the fabrication of TiO_2/$Cu_2ZnSn(S, Se)_2$ solar cells indicated that the kesterite crystal was successfully synthesized, based on Cu-poor Cu/(Zn+Sn) = 0.86 and Zn-rich Zn/Sn = 1.25, which were used as the basis for the precursor ratio calculations. The synthesized solutions of CZTS and CZTSSe made locally are physically orange, while those made from standard are light blue and dark blue-black.

Crystallinity analysis of CZTS-L, CZTS-N, CZTSSe-L, and CZTSSe-N semiconductors was carried out using the reference intensity ratio (RiR) method. The secondary phases formed include Cu_2S, Cu_2Se, Cu_2SnS_3, Cu_2SnSe_3, ZnS, ZnSe, SnS, SnSe, SnS_2, $SnSe_2$. All the samples made had crystallinity between 17.40 and 31.97%. CZTSSe L produced the best crystallinity of 31.97%, while CZTSSe N produced the lowest crystallinity of 17.40%. 68.0-82.6% amorphous in the absorber layer in this experiment was caused by the treatment without H_2S sulfurization. CZTSSe N also had the lowest percentage of secondary phase (16.2%) among the samples. CZTS produced a secondary phase of $Cu_2(S/Se)$, which was more dominant than the CZTSSe phase. The results showed that Se atoms could bind Cu more strongly, producing a kesterite structure with higher crystallinity than S atoms. The higher Cu elementary ratio values also strengthened it in CZTS compared to CZTSSe. Local materials produced higher $Cu_2Sn(S/Se)_3$ and Sn(S/Se) secondary phases than standard materials. The lack of dissolved Zn atoms in the synthesis process made it easy for Cu-Zn-S/Se atoms to form a secondary phase.

Material grain-size data supported the morphological analysis of kesterite crystals using XRD-based FWHM analysis. The surface morphology of the CZTS absorber thin film was for the four samples: CZTS-L, CZTS-N, CZTSSe-L, and CZTSSe-N. It could be concluded that the CZTS L sample has a uniform shape with CZTSSe L in sheet form. At the same time, CZTS N has a uniform shape, whereas CZTSSe N is round and smaller than the local materials. The addition of Se atoms to CZTS leads to a 2-3-fold decrease in grain size in both local and standard materials. The grain size of CZTS L was originally 195.9 nm to 98.1 nm. Meanwhile, the grain size of CZTS N was originally 32.8 nm to 10.7 nm.

Analysis of the optical characteristics of $TiO_2/Cu_2ZnSn(S, Se)_2$ solar cells found that the CZTS synthesis solution has a main peak at a wavelength of 300-308 nm and a second peak for local materials at 418-423 nm, while the standard material is at 705-713 nm. The addition of Se atoms contributed to the redshift of each peak, which decreased the bandgap by 0.08-0.28 eV. The kesterite addition broadened the absorption range from a maximum at 381 nm in TiO2 to 1069 nm, thereby increasing light-absorption efficiency to 71.68%. The use of Se material in CZTS did not shift the absorption peak of the CZTS absorber layer but managed to increase the average efficiency of light absorption by 0.49-4.07%. The presence of the secondary phase content of $Cu_2Sn(S/Se)_3$ and Sn(S/Se) in the local material is higher than the content of the secondary Phase in the standard material, causing the average LHE of the local material to be lower than that of the standard material.

Analysis of the electronic characteristics of $TiO_2/Cu_2ZnSn(S, Se)_2$ solar cells indicated that the smaller the kesterite grain size, the smaller the kesterite bandgap. The content of the secondary phase $Cu_2Sn(S/Se)_3$ and Sn(S/Se) in the local material impacts the large grain size in CZTS L and CZTSSe L. The formation of pores in the absorber layer with a small grain size will reduce the film's reflectance. Thus, the absorbed light could increase due to the presence of pores. Therefore, CZTSSe N, with the smallest bandgap, contributed the most significant LHE (88.12%) among the samples. As a result, CZTSSe N achieved the highest efficiency among the samples.

On the other hand, the efficiency of CZTSSe L was 92%, close to the efficiency of CZTSSe N. TiO_2/CZTS L solar cells produced the highest Jsc (0.972 $mA.cm^{-2}$), and the low Cu_2S and ZnS secondary phases contributed to the high LHE value at the first peak, thus contributing to reduced recombination and high sample Jsc values. TiO_2/CZTSSe N solar cells achieved the highest Voc and F.F. (0.42 V and 50.5%, respectively). The low energy gap value and small grain size support this data. CZTSSe N has a minor error or is closest to the non-stoichiometric ratio of the expected $Cu_{2.1}Zn_{1.25}SnS_2Se_2$ reference with a standard error of 16.0%. CZTSSe N also has the lowest secondary phase percentage (16.2%) among the samples, thereby contributing to the high Voc and electrical contact.

Acknowledgment

This research is funded by the Universitas Pendidikan Indonesia through the research program of Research Grant for QS Ranking Improvement (RQS) with Contract No. 667/UN40.F7/PT.01.01/2026.

Declaration

Clinical Trial Registration Not applicable. This study is not a clinical trial.

Ethics Approval and Consent to Participate Not applicable. This study did not involve human participants, human data, or animal subjects.

Consent for Publication Not applicable. This manuscript does not contain any individual person's data in any form (including individual details, images, or videos).

Funding This research was financially supported by Universitas Pendidikan Indonesia through the Research Grant for QS Ranking Improvement (RQS) program, under Contract No. 667/UN40.F7/PT.01.01/2026.

Conflicts of Interest The authors declare that they have no known competing financial interests or personal relationships that could have appeared to influence the work reported in this paper.

Data Availability The data that support the findings of this study are available from the corresponding author upon reasonable request.

References

[1] BP, B.P., Google Scholar. There is no corresponding record for this reference—vol**,** (2019) pp.
[2] Indonesıa, S., Jakarta: Statistics Indonesia. vol**,** (2015) pp.
[3] Dogan, E., Seker, F., Renewable and Sustainable Energy Reviews. vol **60,** (2016) pp. 1074-1085.
[4] Fathi, B., Ashena, M., Bahari, A.R., Sustainable Production and Consumption. vol **26,** (2021) pp. 588-596.
[5] Gustafson, A., Marlon, J.R., Goldberg, M.H., Wang, X., Ballew, M.T., Rosenthal, S.A., et al., Environment: Science and Policy for Sustainable Development. vol **62,** 2 (2020) pp. 30-35.
[6] British Petroleum, London, UK. vol**,** (2004) pp.
[7] Inglesi-Lotz, R., Dogan, E., Renewable Energy. vol **123,** (2018) pp. 36-43.
[8] O'Regan, B., Grätzel, M., Nature. vol **353,** 6346 (1991) pp. 737-740.
[9] Prima, E., Nuruddin, A., Yuliarto, B., Kawamura, G., Matsuda, A., New Journal of Chemistry. vol **42,** 14 (2018) pp. 11616-11628.
[10] Prima, E.C., Hidayat, N.N., Yuliarto, B., Suyatman, Dipojono, H.K., Spectrochim Acta Mol Biomol Spectrosc vol **171,** (2017) pp. 112-125.
[11] Hasan, H., Jurnal Riset dan Teknologi Kelautan. vol **10,** (2012) pp. 169-180.
[12] Bachdar, F., Lex Privatum. vol **4,** 3 (2016) pp.
[13] Setyawati, D., Energy Policy. vol **144,** (2020) pp. 111569.
[14] Green, M.A., Englewood Cliffs. vol**,** (1982) pp.
[15] Shockley, W., Queisser, H.J., Journal of Applied Physics. vol **32,** 3 (1961) pp. 510-519.
[16] Chapin, D.M., Fuller, C., Pearson, G., Journal of Applied Physics. vol **25,** 5 (1954) pp. 676-677.
[17] Carp, O., Huisman, C.L., Reller, A., Progress in Solid State Chemistry. vol **32,** 1–2 (2004) pp. 33-177.
[18] Nugroho, H.S., Refantero, G., Septiani, N.L.W., Iqbal, M., Marno, S., Abdullah, H., et al., Journal of Industrial and Engineering Chemistry. vol **105** (2022) pp. 83-110.
[19] Nugroho, H.S., Refantero, G., Prima, E.C., Panatarani, C., Suyatman, Nugraha, N., et al., IOP Conference Series: Materials Science and Engineering. vol **1045,** 1 (2021) pp. 012039.
[20] Eunah, K., Zhong-Tao, J., Kwangsoo, N., Japanese Journal of Applied Physics. vol **39,** 8R (2000) pp. 4820.
[21] Seo, D.-K., Hoffmann, R., Theoretical Chemistry Accounts. vol **102,** 1 (1999) pp. 23-32.
[22] Ito, K., Nakazawa, T., Japanese Journal of Applied Physics. vol **27,** Part 1, No. 11 (1988) pp. 2094-2097.
[23] Rühle, S., Solar Energy. vol **130,** (2016) pp. 139-147.
[24] Shockley, W., J Appl Phys. vol **32,** 3 (1961) pp. 510-519.
[25] Zhang, S., Northrup, J.E., Physical Review Letters. vol **67,** 17 (1991) pp. 2339.
[26] Qian, G.-X., Martin, R.M., Chadi, D., Physical Review B. vol **38,** 11 (1988) pp. 7649.
[27] Yoshikawa, K., Kawasaki, H., Yoshida, W., Irie, T., Konishi, K., Nakano, K., et al., Nature Energy. vol **2,** 5 (2017) pp. 1-8.
[28] Kato, T., Japanese Journal of Applied Physics. vol **56,** 4S (2017) pp. 04CA02.
[29] Vellini, M., Gambini, M., Prattella, V., Energy. vol **138,** (2017) pp. 1099-1111.
[30] Fthenakis, V.M., Renewable and Sustainable Energy Reviews. vol **8,** 4 (2004) pp. 303-334.
[31] Liu, S., Guan, Y., Sheng, Y., Hu, Y., Rong, Y., Mei, A., et al., Advanced Energy Materials. vol **10,** 13 (2020) pp. 1902492.
[32] Raiguru, J., Mahanandia, P., Subudhi, B., Optical Materials. vol**,** (2020) pp. 110612.
[33] Prima, E.C., Wong, L.H., Ibrahim, A., Yuliarto, B., Optical Materials. vol **114,** (2021) pp. 110947.
[34] Prima, E.C., Vitadewi, A., Rahmat, A.D., Suhendi, E., Yuliarto, B., International Journal of Nanoelectronics & Materials. vol **14,** 4 (2021) pp. 357-372.

[35] Refantero, G., Prima, E.C., Setiawan, A., Panatarani, C., Cahyadi, D., Yuliarto, B., Journal of Materials Science: Materials in Electronics. vol **31,** 4 (2020) pp. 3674-3680.
[36] Prawira, Y.Y., Prima, E.C., Refantero, G., Setyo, H., Panatarani, B.Y., International Journal of Nanoelectronics & Materials. vol **13,** 2 (2020) pp. 307-314.
[37] Panatarani, C., Redianti, H., Faizal, F., Cahya Prima, E., Yuliarto, B., Joni, I.M., Key Engineering Materials. vol **860,** (2020) pp. 42-50.
[38] Prima, E.C., Nugroho, H.S., Nugraha, Refantero, G., Panatarani, C., Yuliarto, B., RSC Advances. vol **10,** 60 (2020) pp. 36873-36886.
[39] Prima, E.C., Nuruddin, A., Yuliarto, B., Kawamura, G., Matsuda, A., New Journal of Chemistry. vol **42,** 14 (2018) pp. 11616-11628.
[40] Prima, E.C., Putri, A.R., Rustaman, N., Journal of Science Learning. vol **1,** 2 (2018) pp. 60-70.
[41] Prima, E.C., Yuliarto, B., Suyatman, Dipojono, H.K., Mater. Sci. Forum, vol. 889 (2017), pp. 178–183.
[42] Prima, E.C., Qibtiya, M., Yuliarto, B., Suyatman, Dipojono, H.K., Ionics. vol **22,** 9 (2016) pp. 1687-1697.
[43] Prima, E.C., Yuliarto, B., Suyatman, Dipojono, H.K., AIP Conf Proc. vol **1677,** (2015) pp. 120002.
[44] Cahya Prima, E., Yuliarto, B., Kresno Dipojono, H., Adv. Mater. Res., vol. 1112 (2015), pp. 317–320.
[45] Adhyaksa, G.W.P., Prima, E.C., Lee, D.K., Ock, I., Yatman, S., Yuliarto, B., et al., Adv Energy Mater. vol **4,** 18 (2014) pp. 1400470.
[46] Eka, C.P., Yuliarto, B., Suyatman, S., Adv Mat Res vol **789,** (2013) pp. 167-170.
[47] Pal, K., Singh, P., Bhaduri, A., Thapa, K.B., Solar Energy Materials and Solar Cells. vol **196,** (2019) pp. 138-156.
[48] Todorov, T.K., Reuter, K.B., Mitzi, D.B., Advanced Materials. vol **22,** 20 (2010) pp. E156-E159.
[49] Song, J., Teymur, B., Zhou, Y., Ngaboyamahina, E., Mitzi, D.B., ACS Applied Energy Materials. vol **4,** 1 (2021) pp. 81-87.
[50] Akhavan, V.A., Goodfellow, B.W., Panthani, M.G., Steinhagen, C., Harvey, T.B., Stolle, C.J., et al., Journal of Solid State Chemistry. vol **189,** (2012) pp. 2-12.
[51] Martin, N.M., Platzer-Björkman, C., Simonov, K., Rensmo, H., Törndahl, T., Physica Status Solidi (b). vol**,** (2020) pp. 2000308.
[52] Mkawi, E., Al-Hadeethi, Y., Shalaan, E., Bekyarova, E., Ceramics International. vol**,** (2020) pp.
[53] Walsh, A., Chen, S., Gong, X., Wei, S.H. Crystal structure and defect reactions in the kesterite solar cell absorber Cu 2 ZnSnS 4 (CZTS): theoretical insights. AIP Conference Proceedings: American Institute of Physics; 2011. p. 63-64.
[54] Huang, T.J., Yin, X., Qi, G., Gong, H., Physica Status Solidi (RRL)–Rapid Research Letters. vol **8,** 09 (2014) pp. 735-762.
[55] Wang, Z.-S., Kawauchi, H., Kashima, T., Arakawa, H., Coordination Chemistry Reviews. vol **248,** 13 (2004) pp. 1381-1389.
[56] Wang, J., Zhang, P., Song, X., Gao, L., RSC Advances. vol **4,** 41 (2014) pp. 21318-21324.
[57] Wang, D., Liu, L., Basu, N., Zhuang, H.L., Advanced Theory and Simulations. vol **3,** 11 (2020) pp. 2000195.
[58] Wang, W., Winkler, M.T., Gunawan, O., Gokmen, T., Todorov, T.K., Zhu, Y., et al., Advanced energy materials. vol **4,** 7 (2014) pp. 1301465.
[59] Purwanto, H.S., Harjanto, A., Rizkianto, Y., Fatchurohman, D. vol**,** (2019) pp.
[60] Widhiyatna, D., Ernowo, E., Hilman, P.M., Rosana, M.F. Pemanfaatan Metode Analisis Spasial Likelihood Ratio dalam Penentuan Wilayah Prospek Mineralisasi Emas dan Perak Tipe Hidrotermal di Kabupaten Cianjur dan Sukabumi, Provinsi Jawa Barat. Seminar Nasional Geomatika2019. p. 343-356.
[61] Indonesia, "Undang-Undang No. 4 Tahun 2009 tentang Pertambangan Mineral dan Batubara: Justika Siar Publika; (2009) pp.
[62] Prima, E.C., Yuliarto, B., Suyatman, Dipojono, H.K., J Phys Conf Ser vol **739,** 1 (2016) pp. 012031.
[63] Prima, E.C., Utari, S., Chandra, D.T., Hasanah, L., Rusdiana, D., JOTSE: Journal of technology and science education. vol **8,** 4 (2018) pp. 453-472.
[64] Choubrac, L., Lafond, A., Guillot-Deudon, C., Moëlo, Y., Jobic, S., Inorganic chemistry. vol **51,** 6 (2012) pp. 3346-3348.
[65] Shin, B., Gunawan, O., Zhu, Y., Bojarczuk, N.A., Chey, S.J., Guha, S., Progress in Photovoltaics: Research and Applications. vol **21,** 1 (2013) pp. 72-76.
[66] Brammertz, G., Buffière, M., Oueslati, S., El Anzeery, H., Ben Messaoud, K., Sahayaraj, S., et al., Applied Physics Letters. vol **103,** 16 (2013) pp. 163904.
[67] Vanalakar, S., Shin, S., Agawane, G., Suryawanshi, M., Gurav, K., Patil, P., et al., Ceramics International. vol **40,** 9 (2014) pp. 15097-15103.
[68] Li, C., Yao, B., Li, Y., Xiao, Z., Ding, Z., Zhao, H., et al., Journal of Alloys and Compounds. vol **643,** (2015) pp. 152-158.
[69] Pulgarín-Agudelo, F., Vigil-Galán, O., Nicolás-Marín, M., Courel, M., González, R., Mendoza-León, H., et al., Materials Research Express. vol **4,** 12 (2017) pp. 125501.
[70] Ashfaq, A., Jacob, J., Bano, N., Nabi, M.A.U., Ali, A., Ahmad, W., et al., Ceramics International. vol **45,** 8 (2019) pp. 10876-10881.
[71] Ali, A., Jacob, J., Arshad, M.I., un Nabi, M.A., Ashfaq, A., Mahmood, K., et al., Solid State Sciences. vol**,** (2020) pp. 106198.

[72] Mendis, B.G., Goodman, M.C., Major, J.D., Taylor, A.A., Durose, K., Halliday, D.P., Journal of Applied Physics. vol **112,** 12 (2012) pp. 124508.
[73] Vigil-Galán, O., Courel, M., Espindola-Rodríguez, M., Jiménez-Olarte, D., Aguilar-Frutis, M., Saucedo, E., Solar Energy Materials and Solar Cells. vol **132,** (2015) pp. 557-562.
[74] Liu, W.-S., Chen, S.-Y., Huang, C.-S., Lee, M.-Y., Kuo, H.-C., Journal of Alloys and Compounds. vol **853,** (2021) pp. 157237.
[75] Patterson, A., Physical Review. vol **56,** 10 (1939) pp. 978.
[76] Scherrer, P. Bestimmung der inneren Struktur und der Größe von Kolloidteilchen mittels Röntgenstrahlen. Kolloidchemie: Ein Lehrbuch. Springer (1912). pp. 387-409.
[77] Kumar, Y.K., Bhaskar, P.U., Babu, G.S., Raja, V.S., Physica Status Solidi (a). vol **207,** 1 (2010) pp. 149-156.
[78] Bhosale, S., Suryawanshi, M., Kim, J., Moholkar, A., Ceramics International. vol **41,** 7 (2015) pp. 8299-8304.
[79] Katagiri, H., Jimbo, K., Tahara, M., Araki, H., Oishi, K., MRS Online Proceedings Library Archive. vol **1165,** (2009) pp.
[80] Katagiri, H., Jimbo, K., Maw, W.S., Oishi, K., Yamazaki, M., Araki, H., et al., Thin Solid Films. vol **517,** 7 (2009) pp. 2455-2460.
[81] Guo, M., Chen, J., Zhang, J., Su, H., Liu, L., Fu, N., et al., Electrochimica Acta. vol **263,** (2018) pp. 373-381.
[82] Tauc, J., Materials Research Bulletin. vol **3,** 1 (1968) pp. 37-46.
[83] Tauc, J., Grigorovici, R., Vancu, A., Physica Status Solidi (b). vol **15,** 2 (1966) pp. 627-637.
[84] Dzade, N.Y., Scientific Reports. vol **11,** 1 (2021) pp. 1-11.
[85] Hadke, S.H., Levcenko, S., Lie, S., Hages, C.J., Márquez, J.A., Unold, T., et al., Advanced Energy Materials. vol **8,** 32 (2018) pp. 1802540.
[86] Su, Z., Tan, J.M.R., Li, X., Zeng, X., Batabyal, S.K., Wong, L.H., Advanced Energy Materials. vol **5,** 19 (2015) pp. 1500682.